Acta Pharmaceutica Sinica B 2019;9(3):575–589

Chinese Pharmaceutical Association
Institute of Materia Medica, Chinese Academy of Medical Sciences

Acta Pharmaceutica Sinica B

www.elsevier.com/locate/apsb
www.sciencedirect.com

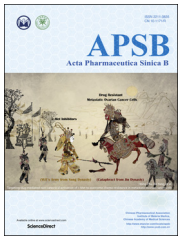

ORIGINAL ARTICLE

Neutrophil-mimicking therapeutic nanoparticles for targeted chemotherapy of pancreatic carcinoma

Xi Cao, Ying Hu, Shi Luo, Yuejing Wang, Tao Gong, Xun Sun, Yao Fu*, Zhirong Zhang*

Key Laboratory of Drug Targeting and Drug Delivery Systems, Ministry of Education, West China School of Pharmacy, Sichuan University, Chengdu 610041, China

Received 16 September 2018; received in revised form 26 October 2018; accepted 20 December 2018

KEY WORDS

Naïve neutrophils membrane;
Celastrol;
PEG-PLGA nanoparticle;
Pancreatic carcinoma;
Inflammation

Abstract Due to the critical correlation between inflammation and carcinogenesis, a therapeutic candidate with anti-inflammatory activity may find application in cancer therapy. Here, we report the therapeutic efficacy of celastrol as a promising candidate compound for treatment of pancreatic carcinoma *via* naïve neutrophil membrane-coated poly(ethylene glycol) methyl ether-*block*-poly(lactic-*co*-glycolic acid) (PEG-PLGA) nanoparticles. Neutrophil membrane-coated nanoparticles (NNPs) are well demonstrated to overcome the blood pancreas barrier to achieve pancreas-specific drug delivery *in vivo*. Using tumor-bearing mice xenograft model, NNPs showed selective accumulations at the tumor site following systemic administration as compared to nanoparticles without neutrophil membrane coating. In both orthotopic and ectopic tumor models, celastrol-loaded NNPs demonstrated greatly enhanced tumor inhibition which significantly prolonged the survival of tumor bearing mice and minimizing liver metastases. Overall, these results suggest that celastrol-loaded NNPs represent a viable and effective treatment option for pancreatic carcinoma.

Abbreviations: 5-FU, fluorouracil; CLT, celastrol; DAPI, 4′,6-diamidino-2-phenylindole; DiD, 1,1′-dioctadecyl-3,3,3′,3′-tetramethylindodicarbocyanine perchlorate; IKKα, IκB kinase α; IKKβ, IκB kinase β; IL-1β, interleukin 1 beta; IL-6, interleukin 6; NF-κB, nuclear factor kappa B; NIK, NF kappa B inducing kinase; NNPs, neutrophil membrane-coated nanoparticles; NPs, nanoparticles without neutrophil membrane coating; PEG-PLGA, poly(ethylene glycol) methyl ether-*block*-poly(lactic-*co*-glycolic acid); PI, propidium iodide; TAK1, TGF-β-activated kinase 1; TEM, transmission electronic microscopy; TNF-α, tumor necrosis factor alpha

*Corresponding authors. Tel.: +86 28 65503798 (Yao Fu), +86 28 85501566 (Zhirong Zhang); fax: +86 28 85501615.
E-mail addresses: yfu4@scu.edu.cn (Yao Fu), zrzzl@vip.sina.com (Zhirong Zhang).

Peer review under responsibility of Institute of Materia Medica, Chinese Academy of Medical Sciences and Chinese Pharmaceutical Association.

https://doi.org/10.1016/j.apsb.2018.12.009

1. Introduction

Pancreatic cancer is the 3rd leading cause of cancer-related mortality in the United States, and over 53,000 people were diagnosed with pancreatic cancer in the year of 2015[1,2]. Often, patients with pancreatic cancer failed to be diagnosed until the disease reaches an advanced stage due to asymptomatic conditions[3]. Pancreatic cancer aggressively metastasizes to adjacent organs or tissues including lymph nodes, liver, peritoneal cavity, large intestines or lung thus resulting in very limited clinical treatment options besides surgery and chemotherapy[4,5]. Depending on the stage and metastasis of the tumor, surgical intervention is only possible in about 15% to 20% of the cases[1,6]. Chemotherapy with gemcitabine, fluorouracil (5-FU) or a combo with nanoparticle albumin-bound paclitaxel (Nab-paclitaxel) are recommended as standard treatment options with serious adverse effects among patients[7,8]. Overall, effective yet safe therapeutic options are still lacking.

Over the past decade, the connection between inflammation and tumorigenesis has gradually been recognized in various pathological contexts such as esophageal cancer after Barrett's metaplasia, colorectal cancer after inflammatory bowel disease, ulcerative colitis and Crohn's disease or pancreatic ductal adenocarcinoma after chronic pancreatitis[9–11]. Regarding the pathogenesis of acute or chronic pancreatitis, activation of nuclear factor kappa B (NF-κB) has been an early response to inflammation in the experimental model of pancreatitis resulting in the secretion of pro-inflammatory cytokines such as tumor necrosis factor-α (TNF-α) and interleukin-1β (IL-1β)[12–14]. Increased mitogenic signals create a selective pressure to acquire mutations favoring survival or uncontrolled proliferation which may further lead to carcinogenesis[15]. Thus, therapeutics specifically inhibiting NF-κB may be explored as antitumor candidates for the treatment of pancreatic cancer. Celastrol (CLT) is a pentacyclic triterpenoid extracted from traditional Chinese medicine, *Tripterygium wilfordii* Hook. f., which displays superior anti-inflammatory activity by inhibiting NF-κB activation in multiple inflammation disease models[12,16–18]. CLT has also been shown to display extensive antitumor activity against various cancers including acute promyelocytic leukemia, hepatocellular carcinoma, osteosarcoma, melanoma, gastric cancer, pancreatic cancer, and colon cancer[19]. Our previous work reported a CLT-derived compound to achieve targeted therapy against severe acute pancreatitis (AP) *via* a *N*, *N*-dimethyl-1,2-diaminoethane moiety[12]. However, delivering therapeutic cargos selectively to the pancreas following systemic administration has always remained a great challenge for targeted therapy of pancreatic diseases.

Neutrophils as the early leukocytes recruited to an inflammatory site provide the first line of defense from innate immune system against infections[20–22]. Recently, the application of neutrophils as therapeutic vehicles in cancer therapy has gradually been recognized. Zhang et al.[23] reported a neutrophil-based delivery strategy for suppression of postoperative malignant glioma recurrence using live neutrophils carrying paclitaxel-loaded liposomes. Meanwhile, Kang et al.[24,25] highlighted the use of activated neutrophil membrane-coated nanoparticles targeting to circulating tumor cells in the treatment of metastatic breast tumor. Instead of using viable cells, cell plasma membrane-camouflaged nanoparticles offer a unique platform technology to achieve site-specific delivery of therapeutic cargos in the treatment of cancer and inflammatory diseases[26–29]. Herein, we hypothesize that the naïve neutrophil plasma membrane should endow therapeutic nanoparticles the neutrophil-like profiles which can be recruited by chemokines, and driven to the tumor site[30]. In this study, CLT-loaded PEG-PLGA nanoparticles were synthesized, coated with naïve neutrophil membrane, and explored for the targeted therapy of pancreatic adenocarcinoma in animal models.

2. Materials and methods

2.1. Materials, cells and animals

Celastrol (CLT) was bought from Chengdu Must Biotechnology (Chengdu, China). PEG-PLGA (PEG average MW 5000 Da; PLGA 50:50, MW 45,000–75,000 Da) was synthesized by Dr Jianyuan Hao from Electronic Film and Materials Laboratory at the University of Electronic Science and Technology of China (Chengdu, China). Solutol HS15 was obtained from BASF (Ludwigshafen, Germany). 3-[4,5-Dimethylthiazol-2-yl]-2,5-diphenyl tetrazolium bromide (MTT) and 1,1′-dioctadecyl-3,3,3′,3′-tetramethylindodicarbocyanine perchlorate (DiD) were provided by Sigma–Aldrich (St. Louis, MO, USA). 4′,6-Diamidino-2-phenylindole (DAPI) was bought from Beyotime (Haimen, China). All other reagents and chemicals used were of analytical grade.

Murine RAW264.7 macrophages, murine Panc02 pancreatic cancer cells, L929 mouse fibroblasts and human umbilical vein endothelial cells (HUVEC) were purchased from the Shanghai Institutes for Biological Sciences. Panc02 cells with standard green fluorescent protein (GFP) expression were obtained from Keyuandi Biotech (Shanghai, China). RAW264.7, Panc02 and B16F10 cells were maintained in RPMI 1640 culture media supplemented with 10% fetal bovine serum (Gibco, USA), 100 U/mL penicillin, and 100 μg/mL streptomycin at 37 °C in a humidified atmosphere containing 5% CO_2.

Female C57BL/6 mice (20 ± 2 g) and male Sprague–Dawley rats (200 ± 20 g) were purchased from Sichuan People's Hospital (Chengdu, China) and maintained under standard housing conditions. All animal protocols were performed in accordance with institutional guidelines, and approved by the Ethics Committee of Sichuan University.

2.2. Isolation of peripheral neutrophils and membranes

First, 20 mL of whole blood was collected from male Sprague–Dawley rats by cutting femoral artery. Next, naïve neutrophils were collected from using a neutrophil collection kit (Haoyang TBD science, Tianjin, China) per the manufacturer's protocol.

In brief, cells were suspended in 10 mL hypotonic lysis buffer. The buffer was consisted of potassium chloride (KCl), magnesium chloride ($MgCl_2$), as well as one ethylene diamine tetraacetic acid (EDTA)-free mini protease inhibitor tablet (Selleck, Shanghai, China), and further broken using a homogenizer. The entire solution underwent 25 passes before spinning down at 3200 × *g* (Allegra X-22R centrifuge, Beckman Coulter, USA), 4 °C, for 6 min. The supernatant was saved while the pellet was resuspended in lysing buffer and underwent another 20 passes and spun down again. The supernatants were pooled and centrifuged at 20,000 × *g*, 4 °C, for 20 min, after which the pellet was thrown away and the supernatant was centrifuged again at 100,000 × *g*, 4 °C, for 2 min. The pellet containing the plasma membrane was washed with 10 mmol/L pH7.5. Tris(hydroxymethyl)aminomethane-hydrogen chloride (Tris–HCl) and 1 mmol/L EDTA. The final pellet was collected and to be purified neutrophil plasma membrane for the following experiments.

2.3. Preparation PEG-PLGA NPs with different sizes and targeting efficiency to pancreas

PEG-PLGA NPs were synthesized using an emulsion/solvent evaporation method as previously described[13]. In brief, 20 mg of PEG-PLGA copolymer and CLT (10 mg)/DiD (250 μg) were dissolved in 1 mL of chloroform, which was then added with deoxycholic acid sodium and Solutol HS15 mixed aqueous solution. The mixture was then emulsified by probe sonication (Xinyi, Ningbo, China) on ice bath. Next, we prepared nanoparticles of different size distributions by varying the intensity and time of ultrasonication. PEG-PLGA NPs with an average size of 60 nm (NP60) was prepared by probe sonication (Xinyi, Ningbo, China) on ice bath (400 W, 180 s). PEG-PLGA NPs with an average size of 150 nm (NP150) was prepared by probe sonication on ice bath (240 W, 80 s), while PEG-PLGA NPs with an average size of 300 nm (NP300) was obtained by probe sonication at 200 W for 50 s. Next, chloroform was evaporated under reduced pressure at 40 °C. NNPs was obtained by coating PEG-PLGA NPs with neutrophil plasma membrane *via* a direct extrusion method[21,32,33].

2.4. Preparation and characterization of NNPs

To prepare neutrophil membrane vesicles, membrane materials obtained were physically extruded for 11 passes through a 400 nm polycarbonate membrane. The resulting vesicles were then coated onto PEG-PLGA cores by co-extruding vesicles and cores through a 220 nm polycarbonate membrane (Sigma–Aldrich). To optimize the membrane-to-NPs ratio, NNPs were composed at membrane to NPs weight ratios ranging from 0 to 2.8 mg of protein per 1 mg of PEG-PLGA. PEG-PLGA nanoparticle cores without membrane coating were used as control. Particle sizes were determined in triplicate by dynamic light scattering analysis (Malvern, NanoZS90, UK), after adjusting the solution to 1 × PBS, and over time for a period of 2 days in 1 × PBS.

To determine the decoration of the neutrophil membrane, the particle size as well as ζ-potential of NNPs was determined by Malvern Zetasizer (Malvern, NanoZS90, UK). The morphology was observed using transmission electron microscopy (TEM, JEM-100CX, JEOL, Japan) after negative fixation with a drop of 1% (*w/v*) uranyl acetate solution.

2.5. Characterization of plasma membrane proteins

To characterize and compare membrane-associated proteins on the freshly obtained neutrophil membrane and NNPs, samples were reduced by 5 mmol/L dithiolthreitol (Sigma–Aldrich), and cysteine residues were alkylated by 10 mmol/L iodoacetamide (Sigma–Aldrich), and then subjected to desalting column purification or ethanol precipitation. Protein samples were then digested with trypsin (Promega, Madison, WI, USA). Then a dissolved peptide was analyzed by nanoLC–ESI-MS/MS (Agilent, Santa Clara, CA, USA), which consisted of a high-pressure liquid chromatography (HPLC, Agilent) with an in house packed reverse phase C18 capillary column (75 μm I.D. × 8 cm, 3 μm in particle size, 300 Å in pore size). Solvent system consisted of solvent A (97.5% *v/v* water, 2% *v/v* acetonitrile, 0.5% *v/v* formic acid) and solvent B (9.5% *v/v* water, 90% *v/v* acetonitrile, 0.5% *v/v* formic acid). Gradient elution was started from 2% *v/v* solvent B to 90% *v/v* solvent B within 60 min. The flow rate was set at 800 nL/min. The injection sample volume was 3 μL. The HPLC system was coupled to a linear ion trap mass spectrometer (LTQ, Thermo, San Jose, CA, USA) in a way that a sample was then ionized by an electrospray ionization process and then got into the mass spectrometer. The ionization voltage was optimized in about 1.5–1.8 kV. The capillary temperature was set at 100 °C.

2.6. Stability and in vitro release

The release profiles CLT and DiD from NPs and NNPs were studied using a standard dialysis setup. In brief, 4 mL of NNPs/CLT and NNPs/Did were placed in dialysis tubes (MWCO 8000 Da), which were subjected to dialysis against 40 mL of 1 × pH 7.4 PBS and 0.2% (*w/v*) Tween 80. The dialysis tubes were gently shaken at 100 rpm at 37 °C. At given time points, 1 mL of sample from the buffer was collected and replaced with 1 mL of fresh buffer. The concentrations of CLT was determined by liquid chromatography–mass spectrometry (LC–MS) analysis. The mobile phase consisted of acetonitrile and 0.5% formic acid (80:20, *v/v*). At a flow rate of 0.4 mL/min, the total run time was about 4.5 min. The DiD concentrations were determined by fluorescence spectroscopy using an RF-5301PC spectrofluorophotometer (Shimadzu, Japan). The excitation wavelength was 647 nm and the emission wavelength was 664 nm. The cumulative drug release percentage was calculated as previously described[31].

2.7. Cell uptake

RAW264.7, HUVEC, L929 cells were seeded in 12-well plates (Corning, NY, USA) at a density of 2×10^5 cells per well and incubated for 24 h at 37 °C. RAW264.7 cells were incubated with or without 10 μg/mL LPS for 48 h prior to incubation with DiD, NPs/DiD, and NNPs/DiD. To perform cell uptake studies, cells were incubated for 1, 2, and 4 h with free DiD solution, NPs/DiD, and NNPs/DiD at an equivalent dose of 1 μg/mL of DiD, respectively. At given time points, cells were harvested, washed, fixed, and subjected to FACS analysis (Beckman Coulter, Fullerton, CA, USA).

2.8. In vivo antitumor efficacy in orthotopic and ectopic pancreatic cancer model

A total of 40 female C57BL/6 (20 ± 2 g) were used to establish orthotopic pancreatic cancer mice models. The abdomen of each mouse was opened by a 0.5-cm left flank incision after injection of

4% chloral hydrate solution (0.1 mL/10 g, i.p.). First, the pancreas was exteriorized through the incision, and the pancreas was slowly injected with 5×10^5 GFP-Panc02 cells. After injection, the post-operative pancreas was put back into the abdomen. The peritoneum and skin were then closed with a 5-0 vicryl suture. Two-week post inoculation, mice were randomized into the following treatment groups ($n = 10$): (a) vehicle control (NNPs-only); (b) CLT solution (1 mg/kg); (c) NPs/CLT (equivalent to 1 mg/kg of CLT); and (d) NNPs/CLT (equivalent to 1 mg/kg of CLT). Forty days post tumor inoculation, half of the mice were sacrificed, major organs and pancreas from each group were removed and subjected to *ex vivo* imaging using IVIS system. The fluorescence intensity was used to represent remaining tumor cells. Meanwhile, the death time of the remaining mice was recorded to generate a survival curve.

As a comparison, a tumor xenograft mice model was established to evaluate the antitumor efficacy of various CLT-based treatment groups. In brief, 1×10^6 Panc02 cells were inoculated into the right flank of all female C57BL/6 mice (6–8 weeks) subcutaneously. The length and width of the tumor were recorded using a caliper every other day. The tumor volume was calculated using the following equation:

$$\text{Volume} = \left(\text{Length} \times \text{Width}^2\right)/2 \quad (1)$$

The treatment groups were managed similarly as in the orthotopic cancer model. For both orthotopic and ectopic pancreatic cancer models, mice were administered with indicated treatments every seven days after the inoculation of tumor for consecutive four doses. Fifty days post tumor inoculation, mice were sacrificed, and solid tumors were then collected for further analysis.

2.9. Immunohistochemistry and histological analysis

For immunohistochemistry and histological studies, heart, liver, spleen, lung, kidney, pancreatic and tumor tissues were fixed with 10% neutral buffered formalin. Then, paraffin-embedded continuous sections (5 μm) were subjected to hematoxylin and eosin (H&E) staining to examine pathology. Sections of all tissue samples were observed under light microscopy (Zeiss Axiovert 40, Göttingen, Germany). Then, the severity of pancreatitis based on edema, inflammation, leukocyte infiltration, alveolar wall thickening and collapse, vacuolization vascular congestion and destruction of alveolar wall, all of these can be seen. Histological evaluation of pulmonary injury was assessed for interstitial and intraalveolar leukocyte infiltrations, interstitial and intraalveolar edema, and fibrosis as previously described[34].

To explore the relationship between inflammation and cancer, histological analysis was conducted on tissue sections. Interleukin 6 (IL-6), tumor necrosis factor-α (TNF-α), tyrosine kinase receptor 1 (TNK1), nuclear factor κ-inducing kinase (NIK), interleukin-1β (IL-1β) and interleukin-6 receptor/cluster of differentiation 126 (IL-6R/CD126) as proinflammatory cytokines, nuclear factor kappa (NF-κB), inhibitor of nuclear factor κ-B kinase (IKK) as downstream inflammatory factors, and caspase 9 in the pancreas and tumors were stained using corresponding rabbit anti-rat or anti-mouse antibodies (1:200 dilution, Abcam, Cambridge, MA, USA) followed by biotinylated anti-IgG antibodies (ZSGB-BIO, China). Tissue sections were counterstained with hematoxylin for nuclei and observed under light microscopy (Zeiss Axiovert 40CFL, Germany).

2.10. Statistics

Student's *t*-test was performed for comparison between two groups, and one-way ANOVA analysis was conducted for comparing multiple groups followed by a Tukey *post hoc* analysis. All results were presented as mean ± SD. A *P*-value of <0.05 was considered statistically significant.

3. Results

3.1. Synthesis and characterizations of NNPs

CLT-loaded PEG-PLGA nanoparticles (NPs) were synthesized *via* an emulsification method[13]. PEG-PLGA NPs displayed an average size of about 142.7 ± 2.8 nm (Fig. 1C) with a narrow distribution (PDI, 0.178 ± 0.023, Fig. 1A), and the obtained neutrophil plasma membrane vesicles showed an average size of about 183.6 ± 3.7 nm (Fig. 1A and C). The coating of neutrophil plasma membrane was accomplished *via* repeated extrusions[30,31]. Upon fusion of the membrane vesicles with PEG-PLGA NPs, the obtained NNPs showed a slight increase in size distributions with an average size of 167.4 ± 2.6 nm (PDI, 0.215 ± 0.037, Fig. 1A and C). TEM visualization showed the obtained NNPs displayed a typical core-shell structure with a single dimmer layer upon negative staining (Fig. 1B). The thickness of the plasma membrane layer was around 10–20 nm, which is consistent with literature findings[24]. Compared to bare PEG-PLGA NPs, an increase of about 10 mV was observed for ζ potential of NNPs which is close to the level of the membrane vesicles (Fig. 1D). According to previous studies on cell membrane-coated nanoparticles, the membrane coating occurs as a translocation of the plasma membrane bilayer onto the nanoparticle surface, resulting in a right-side-out conformation that allows the membrane to retain its functionality[24]. The encapsulation efficiency of NPs/CLT and NNPs/CLT were found to be 92.4 ± 3.1% and 84.6 ± 3.7%, respectively.

To optimize the membrane coating condition, NNPs were synthesized at membrane-to-core weight ratios ranging from 0 to 2.5 mg of membrane protein per 1 mg of PEG-PLGA particles (Fig. 1E). At lower membrane-to-core ratios, a significant increase in the hydrodynamic radius was observed when nanoparticles were transferred to 1 × PBS likely due to incomplete coverage by exposing the surfaces of the cores, thus resulting in low stability in ionic buffers. The effect was even more pronounced after 48 h, as samples with membrane coverage lower than 1 mg of protein per 1 mg of PEG-PLGA aggregated significantly (Fig. 1E). The lowest membrane-to-core ratio at which the particles maintained size stability over time was around 1 mg of protein per 1 mg of PEG-PLGA. At this ratio, there was minimal size increase within 48 h (Fig. 1E).

To ensure that NNPs retain membrane-associated proteins from neutrophil plasma membrane, we performed a proteomic analysis of membrane-associated proteins. Results showed that no nuclear protein was observed in neutrophil membranes or in NNPs indicating the purification and isolation process was successful. In addition, membrane-associated proteins mainly consisted of proteins found in structure/adhesion, signaling, immunity, transport and metabolism (Fig. 1F). Also, no significant differences in protein abundance were observed between neutrophil membrane and NNPs (Fig. 1F), indicating the repeated extrusion and coating steps did not result in the loss of membrane proteins.

Regarding the release profiles of CLT, free CLT showed rapid release with over 95% cumulative release within 7 h, while by encapsulating CLT into PEG-PLGA NPs and NNPs, the release of CLT from NPs/CLT and NNPs/CLT displayed a dual phase profile with less than 50% CLT cumulative release within 5 h (Supporting Information Fig. S1A). Thus, loading hydrophobic small molecule drugs in nanoparticles could prolong the drug release substantially. However, plasma membrane coating did not impact the release behavior of drugs as compared to NPs without membrane coating. Meanwhile, we investigated the release profiles of DiD from NNPs and NPs, which displayed a low cumulative release ($< 30\%$) within the first 4 h (Fig. S1B). Thereby, the slow

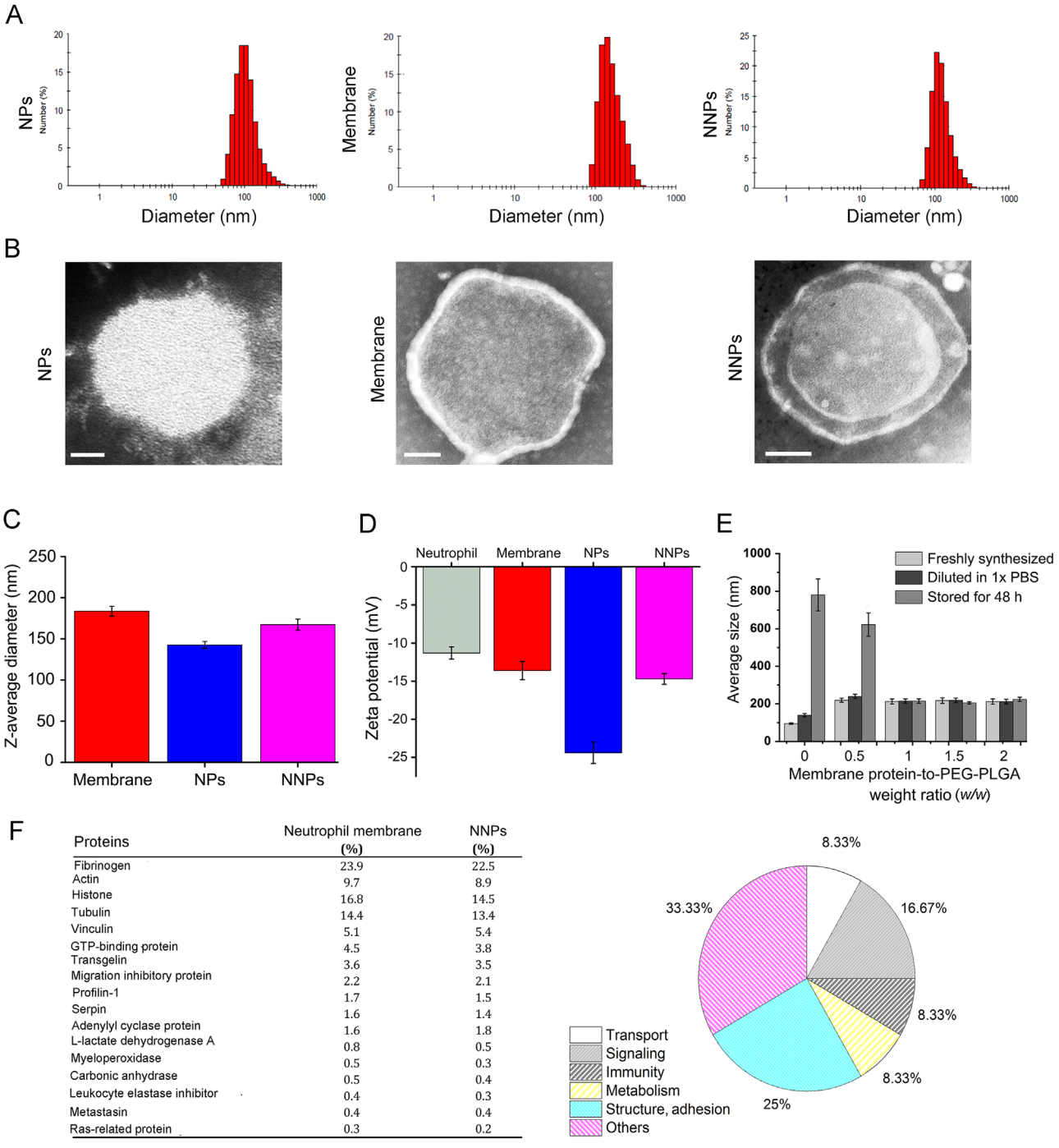

Proteins	Neutrophil membrane (%)	NNPs (%)
Fibrinogen	23.9	22.5
Actin	9.7	8.9
Histone	16.8	14.5
Tubulin	14.4	13.4
Vinculin	5.1	5.4
GTP-binding protein	4.5	3.8
Transgelin	3.6	3.5
Migration inhibitory protein	2.2	2.1
Profilin-1	1.7	1.5
Serpin	1.6	1.4
Adenylyl cyclase protein	1.6	1.8
L-lactate dehydrogenase A	0.8	0.5
Myeloperoxidase	0.5	0.3
Carbonic anhydrase	0.5	0.4
Leukocyte elastase inhibitor	0.4	0.3
Metastasin	0.4	0.4
Ras-related protein	0.3	0.2

Figure 1 Physicochemical characterizations of nanoparticles. (A) Size distributions of NPs, membrane, and NNPs as determined by DLS. (B) TEM images of NPs, membrane, and NNPs. Scale bars represent 30 nm. (C) Hydrodynamic size of PEG-PLGA NPs cores, membrane vesicles, and NNPs. Data represent mean ± SD ($n = 3$). (D) Surface ζ potential of neutrophils, PEG-PLGA NPs cores, membrane vesicles, and NNPs. Data represent means ± SD ($n = 3$). (E) Hydrodynamic size of NNPs as measured by DLS at varying membrane protein to PEG-PLGA weight ratios after adjusting to 1 × PBS, and after storage for 48 h in 1 × PBS. Data represent means ± SD ($n = 3$). (F) Comparative proteomic study of plasma membrane proteins of neutrophils and NNPs.

leaking of DiD from the nanoparticles indicated that DiD-loaded nanoparticles could be used to explore the *in vitro* cellular distribution and the *in vivo* distribution profiles of NPs and NNPs.

3.2. *NNPs enhance cellular uptake efficiency in activated macrophage, HUVEC and Panc02 cells*

Using a near infrared dye as the fluorescence probe, NNPs/DiD markedly increased the uptake efficiency in LPS-stimulated macrophages RAW264.7 as compared to NPs/DiD, while no significant differences in the cellular uptake were observed between NNPs and NPs in RAW264.7 without LPS treatment (Fig. 2A and B). To evaluate the cell uptake of NNPs in endothelial cells, we used HUVECs to perform the uptake study. Interestingly, both NPs/DiD and NNPs/DiD showed time-dependent uptake increase with significantly higher uptake efficiencies for NNPs/DiD at all time points under investigation ($P < 0.05$, Fig. 2C). As suggested in literature, endothelial cells are activated by host inflammatory mediators such as TNF-α which can further mediate the adhesion of neutrophils[32]. Thereby, it is likely that the activation of endothelial cells during

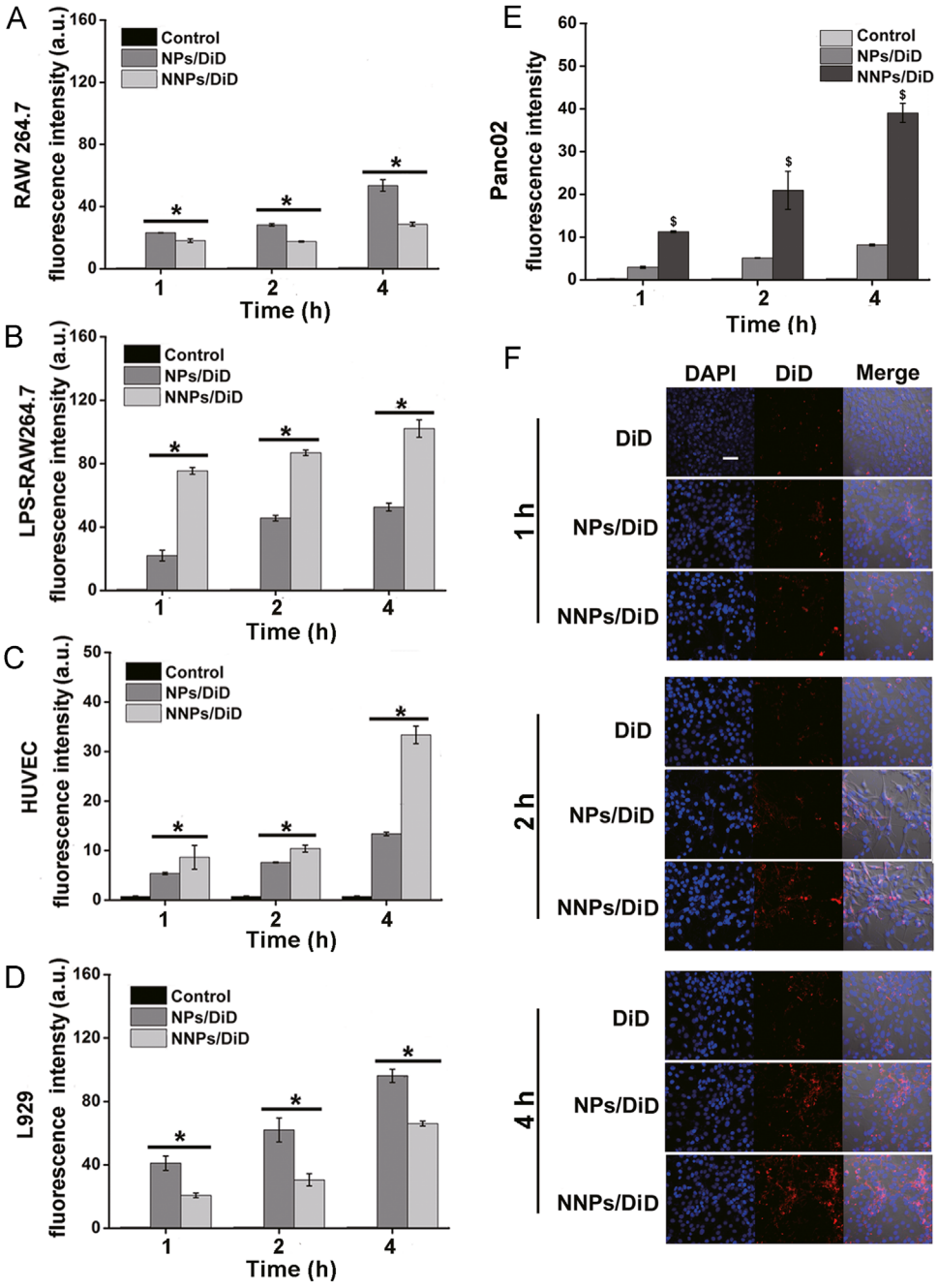

Figure 2 Cellular uptake behaviors in various cell lines. Cellular uptake of NPs/DiD, and NNPs/DiD in (A) murine macrophage RAW264.7, (B) LPS treated RAW264.7, (C) HUVEC, (D) L929; and (E) Panc02 cells at 1, 2, and 4 h. (F) Confocal laser scanning microscopy images of Panc02. Cell nuclei were stained with DAPI (blue) and DiD fluorescence displayed in red. Scale bar represents 100 μm. Data represent mean ± SD ($n=3$). $^{*}P<0.05$ *vs.* NPs/DiD.

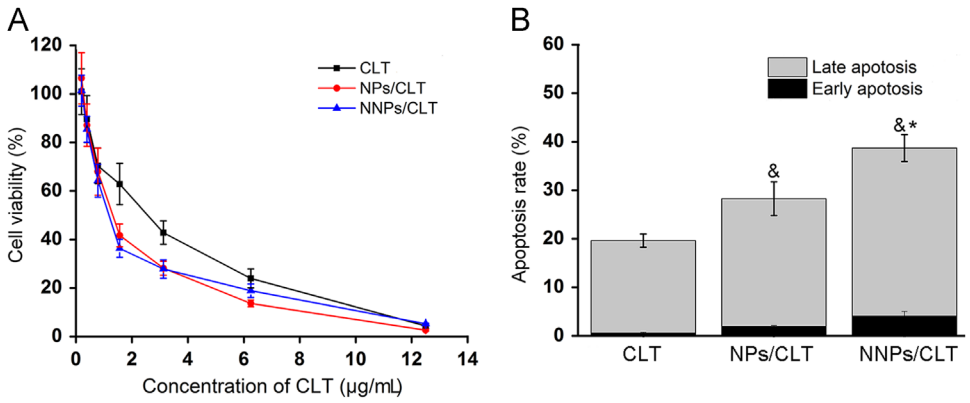

Figure 3 Cytotoxicity and apoptosis. (A) Viability of Panc02 cells after 24 h of treatment of CLT solution, NPs/CLT and NNPs/CLT. (B) Cell apoptosis and necrosis percentages were analyzed by flow cytometry using annexin V-FITC in combination with PI in Panc02 cells after treatment with different formulations. Data represent mean ± SD ($n=3$). $^{\&}P<0.05$ *vs.* CLT, $^{*}P<0.05$ *vs.* NPs/CLT.

inflammation may recruit more NNPs to the site of inflammation. For mouse fibroblast L929, NNPs/DiD decreased the cellular uptake of DiD compared with NPs/DiD (Fig. 2D), which suggests that NNPs is less likely to be taken up by normal cells.

Next, the cell uptake study in Panc02 cells showed that the intracellular fluorescence intensity increased dramatically over time for NPs/DiD and NNPs/DiD groups as compared to DiD solution (Fig. 2E). In comparison, NNPs/DiD displayed significantly higher cellular uptake efficiency than NPs/DiD at each given time point (Fig. 2E). Also, confocal microscopic images showed consistent results regarding cellular uptake over time profiles in Panc02 cells with NNPs/DiD showing the highest DiD fluorescence intensity among all groups under investigation (Fig. 2F).

3.3. *Cytotoxicity and apoptosis study*

In vitro cytotoxicity study indicates CLT solution, NPs/CLT and NNPs/CLT showed dose-dependent inhibition of Panc02 cells, and that encapsulating CLT into nanoparticle formulations exhibited greater inhibitory effect against Panc02 cells than CLT solution after 24 h of treatment (Fig. 3A). Specifically, the IC_{50} values for NNPs/CLT, NPs/CLT and CLT were 0.98, 1.12, 1.58 μg/mL, respectively. Next, we quantified the proportion of apoptotic and necrotic cells by flow cytometry *via* annexin V-FITC and PI double staining. Both NPs/CLT and NNPs/CLT showed significantly higher apoptotic cell percentages than CLT solution ($P < 0.05$, Fig. 3B), indicating encapsulating CLT in nanoparticles may help improve the efficacy of CLT. Moreover, NNPs/CLT displayed significantly higher apoptosis rate than that of either NPs/CLT ($P < 0.05$, Fig. 3B), which is most likely due to enhanced cell uptake efficiency of NNPs in Panc02 cells as described in the previous section. Together, these results suggest that NNPs/CLT appeared to enhance the potency of CLT against Panc02 cells by increasing the internalization efficiency and apoptosis rate.

3.4. *Biodistribution and anticancer effect in ectopic and orthotopic pancreatic cancer models in mice*

3.4.1. *Ectopic cancer model*

A Panc02-bearing mice xenograft model was established to explore the tumor targetability of NNPs and the anticancer effect of NNPs/CLT. First, *in vivo* fluorescence imaging was performed in tumor bearing mice at 1, 6 and 24 h after intravenous injections of DiD solution, NPs/Did and NNPs/Did. Among all three groups, DiD solution displayed extensive distributions throughout the mice with accumulations in the liver and spleen after 1 h (Fig. 4A and B), and in comparison, NPs/DiD and NNPs/DiD showed increased accumulations at the tumor site (Fig. 4B). In addition, DiD solution displayed rapid metabolism and excretion *in vivo*, while NNPs/DiD showed prolonged circulation with significantly higher accumulations in the tumor after 24 h.

Regarding tumor inhibitory effect, the NNPs/CLT showed excellent antitumor efficacy as compared to the saline control, CLT solution and NPs/CLT treated groups, with tumor volumes being the smallest among all treatment groups at all given time points (Fig. 4C, D and F). Moreover, the weight changes of tumor bearing mice across different treatment groups were not significant ($P > 0.05$, Fig. 4E) indicating the CLT based treatments are tolerable in mice and may not result in systemic adverse effects.

3.4.2. *Orthotopic cancer model*

In vivo imaging was performed in orthotopic GFP-Panc02 cancer model after repeated administrations of CLT solution, NPs/CLT, and NNPs/CLT *via* tail-vein injection (Fig. 5A). Mice were sacrificed on day 28, and after opening the abdomen, *ex vivo* imaging showed extensive distributions of tumor cells in the saline group (Fig. 5A), while groups treated with CLT formulations showed much less fluorescence intensity in the peritoneal (Fig. 5A). Also, photo images indicated that the disease conditions of mice in the saline group deteriorated with pancreatic tissues and intestines turning dark (Fig. 5B). Obviously, all CLT formulations dramatically improved the necrosis of viscera in tumor bearing mice (Fig. 5B). Also, *ex vivo* imaging of vital organs and pancreas showed tumor metastasis to the brain in the saline and CLT solution groups, which was not shown in the NPs/CLT and NNPs/CLT groups (Fig. 5C). The fluorescence intensity of the pancreas and the size of pancreas are direct indications of the efficacy of anticancer treatment. NNPs/CLT treated group showed a significant reduction in the fluorescence intensity of the pancreas with the size of pancreas being the smallest among all tumor bearing groups (Fig. 5C–E). NNPs/CLT appeared to significantly prolong the median survival time from 28 days (saline), 35 days (CLT), 38.5 days (NPs/CLT) to 63 days (NNPs/CLT, Fig. 5F).

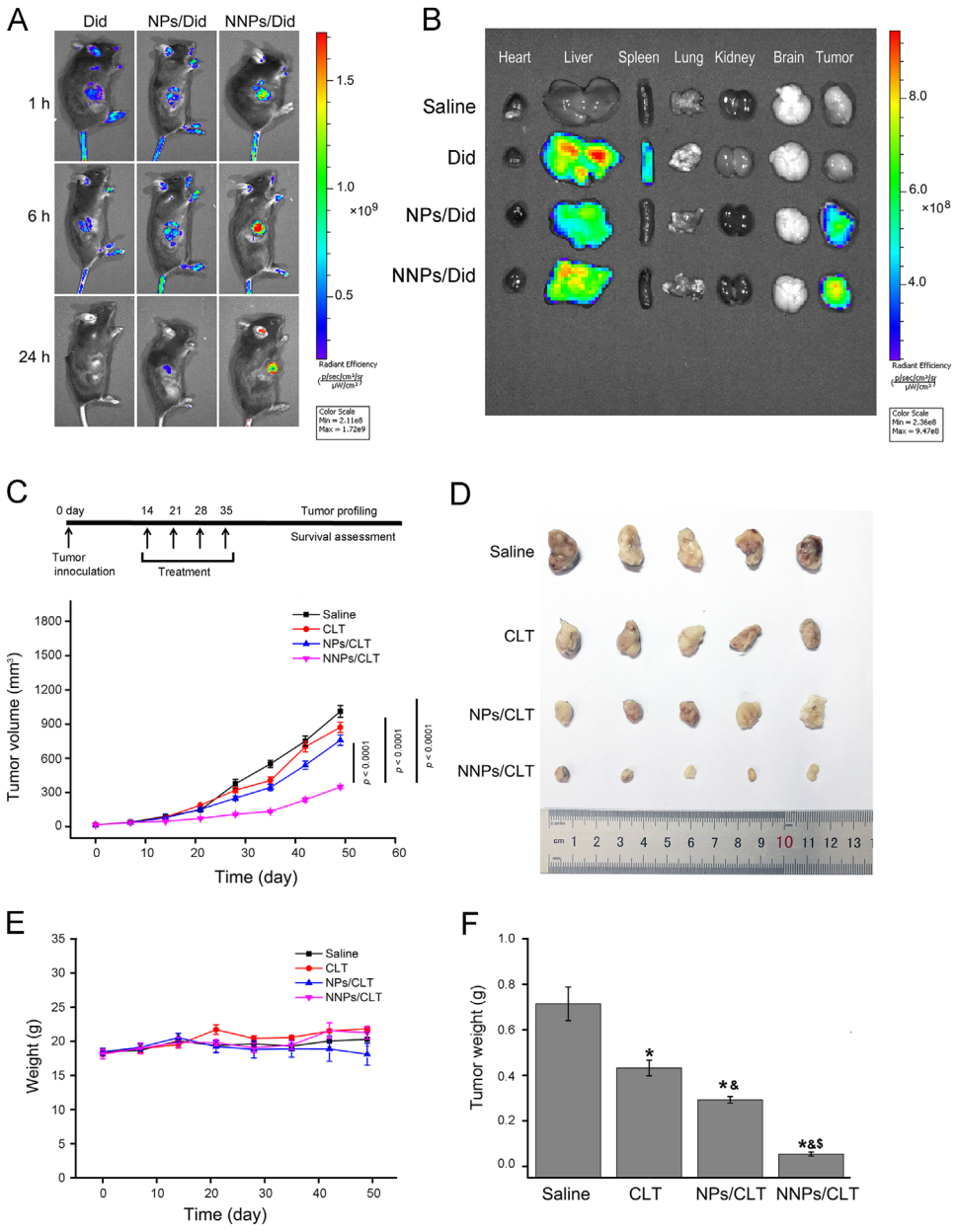

Figure 4 Antitumor efficacy of NNPs/CLT in mice bearing Panc02 xenografts. (A) *In vivo* imaging of tumor bearing mice at 1, 6 and 24 h after i.v. injections of DiD solution, NPs/Did and NNPs/Did. (B) Representative images of vital organs and tumors 24 h after i.v. injections of DiD solution, NPs/Did and NNPs/Did. (C) Dosing regime and average volumes of tumors after different treatments over time. Data represent mean ± SD ($n = 5$). (D) Morphology of tumors in different treatment groups after 35 days. (E) Body weight variations of each treatment group over time. (F) Tumor weight variations of each treatment group over time. Data represent mean ± SD ($n = 5$). $^{*}P < 0.05$ *vs.* normal, $^{\&}P < 0.05$ *vs.* CLT, and $^{\$}P < 0.05$ *vs.* NPs/CLT.

3.5. In vivo toxicity and therapeutic effect in ectopic and orthotopic pancreatic cancer models

Toxicity remains another critical factor to evaluate the potential application of therapeutic agents and formulations. CLT has been reported with systemic adverse effects including cardiotoxicity, and hepatotoxicity[31,33]. For the study using ectopic mice model, tissue histology analysis from H&E staining of major organs revealed no inflammation or cellular damages induced by NNPs/CLT. These results indicated that NNPs/CLT group did not induce systemic toxicity compared with other groups (Fig. 6). But CLT solution shows certain toxicity on heart, liver, spleen, lungs and kidneys. Tissue histology from H&E staining of major organs revealed no inflammation and no cellular damage induced by NNPs/CLT. All these results indicated that NNPs/CLT accumulation occurred in the pancreas and lungs without generating inflammation, suggesting neutrophil membrane represent a safe modification strategy in improving the biocompatibility of synthetic nanoparticles.

For the antitumor study using orthotopic model, NNPs/CLT treatment group showed no obvious toxicity to major organs

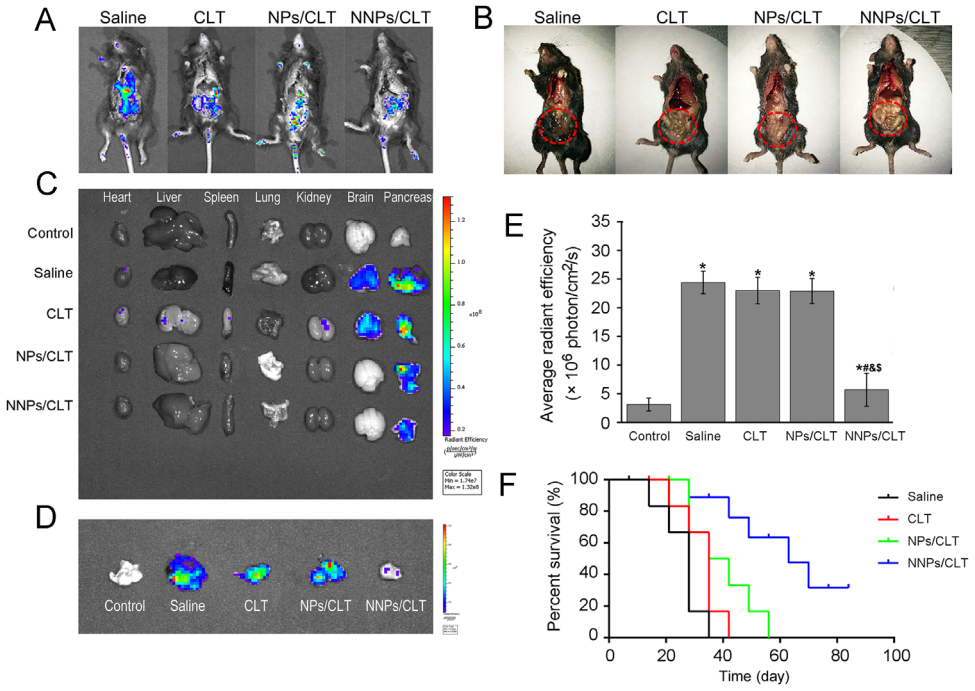

Figure 5 *In vivo* antitumor efficacy in mice bearing GFP-Panc02 orthotopic tumor model. (A) Whole-body fluorescence imaging of mice with surgically open abdomen. Mice were sacrificed on day 35 after indicated treatments. (B) Photo images of the disease conditions after indicated treatment. (C) Representative fluorescence images of vital organs and pancreas. (D) Representative fluorescent images of tumor-bearing pancreas. (E) Semiquantitative analysis of fluorescence intensity of the pancreas. Data represent mean ± SD ($n=5$). $^{*}P<0.05$ *vs.* normal, $^{\#}P<0.05$ *vs.* model, $^{\&}P<0.05$ *vs.* CLT, and $^{\$}P<0.05$ *vs.* NPs/CLT. (F) Survival times in different treatment groups ($n=10$).

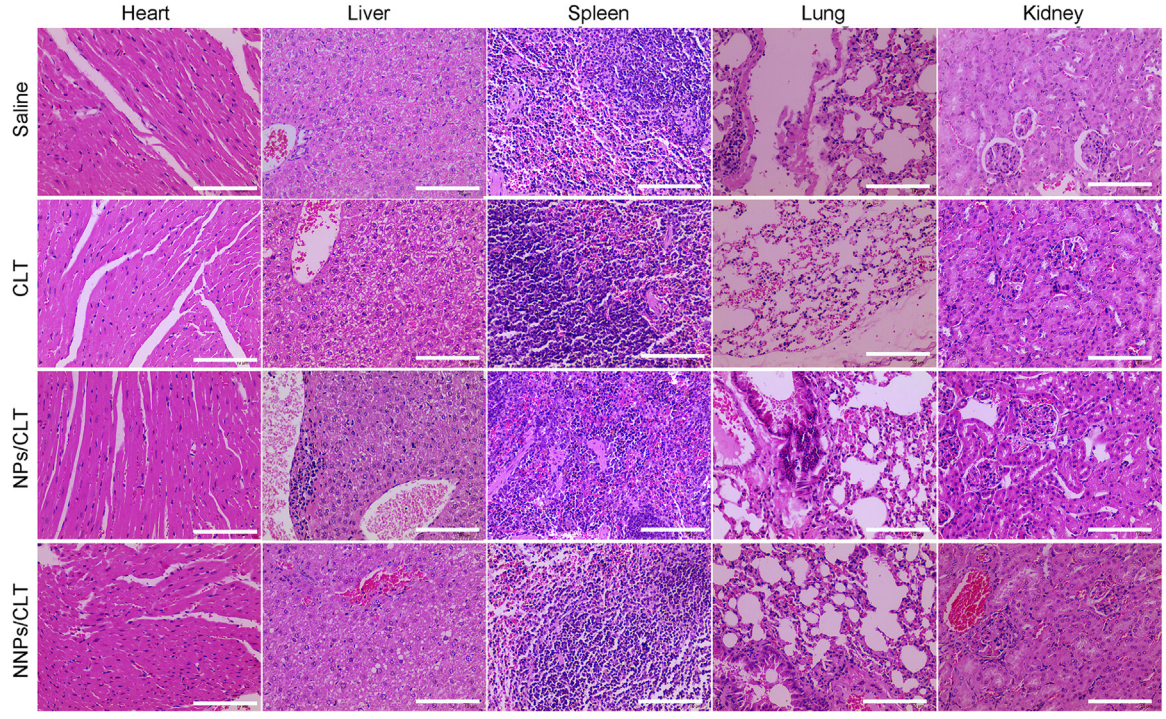

Figure 6 *In vivo* toxicity and therapeutic effect in ectopic pancreatic cancer model. The major organs and tissues were collected for H&E staining and histological analysis. These are representative sections from five mice analyzed for each condition. Scale bar = 100 μm.

compared to CLT solution group. Orthotopic pancreatic cancer models have been reported to develop metastasis to adjacent organs such as liver and gastrointestinal tract[34,35]. In our study, saline, CLT solution, and NPs/CLT all showed obvious liver metastases with dense nuclei clusters representing tumor cells (Fig. 7). Intriguingly, NNPs/CLT treatment group showed greatly reduced liver metastases with the least number of metastatic cancer nests among all treatment groups (Fig. 7).

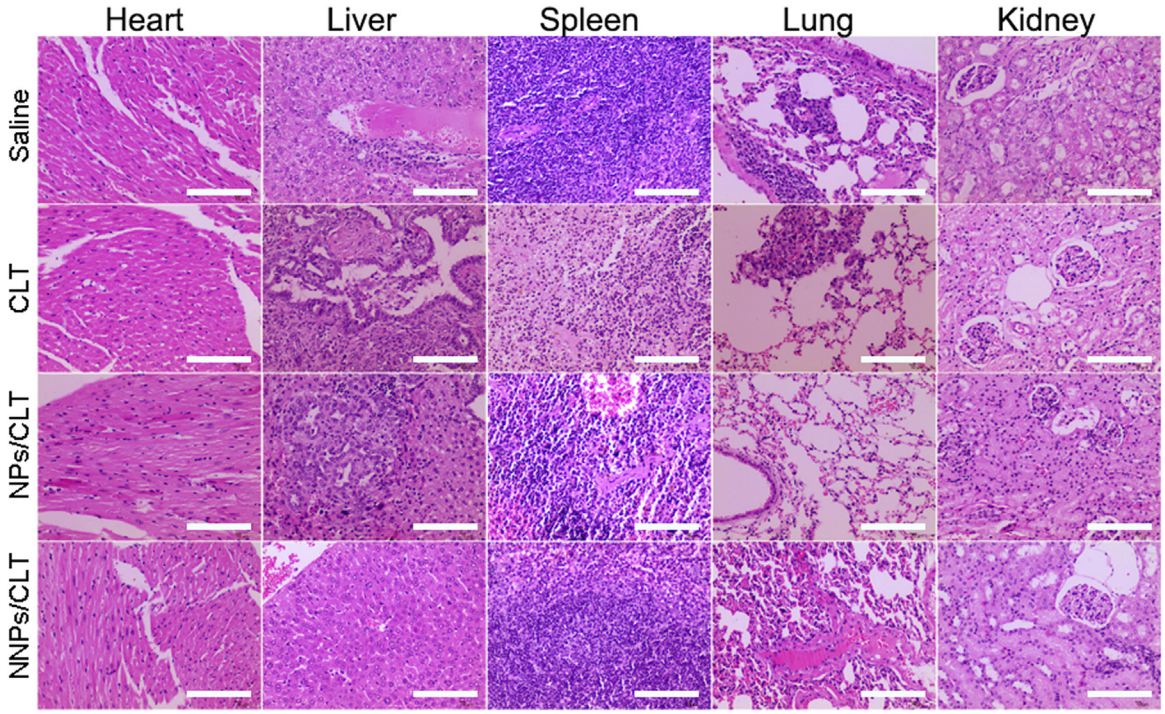

Figure 7 *In vivo* toxicity and therapeutic effect in orthotopic pancreatic cancer model. The major organs and tissues were collected for H&E staining and histological analysis. Liver metastatic nests were pointed out by white arrows. These are representative sections from five mice analyzed for each condition. Scale bar = 100 μm.

3.6. Immunohistochemistry staining of tumor sections in orthotopic and ectopic pancreatic cancer model

Per the immunohistological analysis of tumor sections, the NNPs/CLT-treated group displayed obvious tumor area shrinkage as indicated by fewer tumor cells and more void spaces in the core of tumor tissues, less Ki67 positive cell staining and more TUNEL positive cells in NNPs/CLT treated group (Fig. 8A), indicating the extraordinary antitumor efficacy of NNPs/CLT attributed to the enhanced anti-proliferation and apoptosis-induction effect.

Per the immunohistological analysis of tumor sections, dramatic tumor area shrinkage, less Ki67 positive cell staining and extensive TUNEL positive staining were observed for the NNPs/CLT treated group (Fig. 8B), indicating the extraordinary antitumor efficacy of NNPs/CLT was likely attributed to the greatly enhanced anti-proliferation and pro-apoptosis effect.

3.7. Mechanistic insights into the role of NNPs/CLT to treat pancreatic cancer

Per the immunohistochemistry analysis of both ectopic and orthotopic tumor tissues, results showed obvious downregulation of IL-6, IL-1β and NF-κB in the NNPs/CLT treatment group (Figs. 9 and 10). Consistently, NNPs/CLT treatment appeared to down-regulate the levels of NIK, TAK1, and Ki67 compared with saline and other CLT-based treatment groups (Figs. 8–10), thus indicating a positive anti-inflammatory response in the local tumor environment. According to literature, the tumor inhibitory effect and anti-angiogenesis of CLT has been reported in the treatment of prostate cancers, which is likely mediated through inhibiting the AKT/mTOR signaling pathway[36]. The pharmacological effect of CLT has been well validated in several studies, which is suggested to mainly function by inhibiting NF-κB signaling pathway[36–39]. As NF-κB is actively involved in the proliferation of cancer cells, the inhibition of NF-κB may thus result in anti-proliferation and pro-apoptosis effect.

To gain further insights into the treatment of pancreatic cancer using CLT, possible signaling pathways behind CLT treatment were summarized in Supporting Information Fig. S2. Overexpression of IL-6 and IL-1β have been found to contribute to the pathogenesis of inflammatory diseases as well as cancer[40–42]. As shown in Fig. S2, the downregulation of IL-6 and IL-1β may further impact the downstream factors such as IKK and NF-κB. Notch-mediated IL-6 upregulation was controlled by IKKα and IKKβ, which are inhibitors of NF-κB kinase subunit α and β, respectively, in the NF-κB signaling cascade[43]. Moreover, the transcription factor, NF-κB coordinates the expression of genes that control cell proliferation, survival, and transformation[44]. Thus, strategies that can suppress the activation of NF-κB may show promising therapeutic effects against tumor growth, suggesting NF-κB as a critical therapeutic target for the treatment of pancreatic cancer.

4. Discussion

Due to the malignancy nature of pancreatic cancer and the difficulty to diagnose at an early stage of tumor progression, pancreatic carcinoma remains a leading cause of cancer-related mortality worldwide. Despite advances in cancer chemotherapy, limited treatment options are available for pancreatic cancer, which often result in severe adverse effects and poor patient response[45]. As part of the innate immune defense system, neutrophils are the early cell types recruited to the site of injury through tethering, rolling, crawling and transmigration[46]. The recruiting process

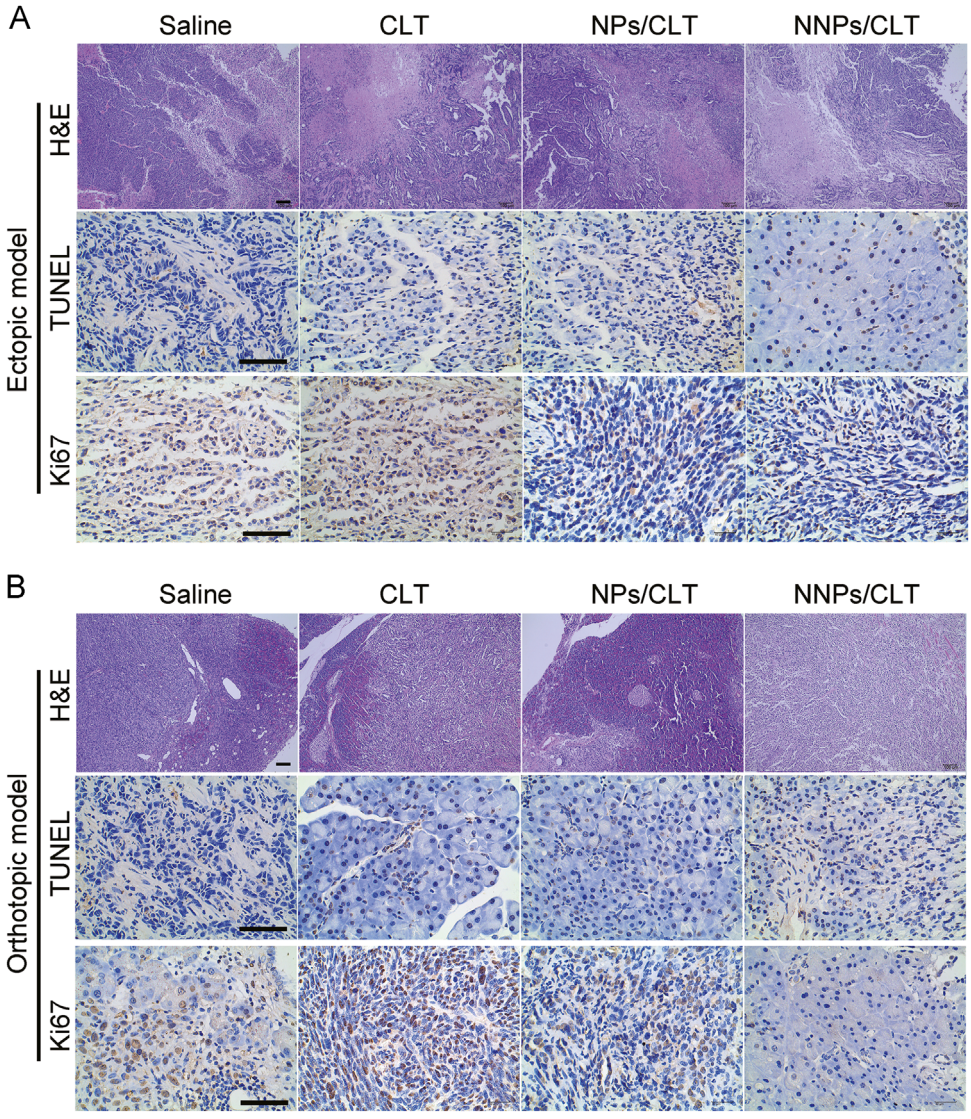

Figure 8 Immunohistochemistry staining of tumor sections of ectopic pancreatic cancer model (A) and orthotopic pancreatic cancer model (B). Scale bars represent 100 μm.

involves the interaction between P-/E-selectin and their glycosylated ligands such as P-selectin glycoprotein ligand 1, and integrin-mediated adhesion[46–48]. Neutrophils have previously been revealed as potent vehicles that can carry nanoparticles or therapeutics to efficiently migrate across blood vessels to reach either the inflammation or the tumor site[23,49]. To improve pancreas-specific drug accumulation, the neutrophil membrane-coating strategy may render therapeutic nanoparticles neutrophil-like properties such as extravasation from blood vessels to the site of tissue injury and chemokine-driven adhesion which may greatly benefit targeted drug delivery to the pancreas. In this work, we fabricated naïve neutrophil membrane-coated PEG-PLGA nanoparticles and explored the therapeutic effect of CLT loaded NNPs for the treatment of pancreatic adenocarcinoma both *in vitro* and *in vivo*.

From the *in vitro* cellular uptake study, NNPs showed significantly enhanced cell internalization efficiency in Panc02, LPS-stimulated RAW264.7 and HUVEC cells compared to nanoparticles without neutrophil membrane coating, which indicates the great potential of NNPs to achieve tumor-selective and inflammation-targeted delivery. In the subsequent studies of apoptosis, NNPs/CLT have been shown to significantly enhance the apoptosis rate of murine Panc02 cells as compared to CLT solution and NPs/CLT. These results further imply that NNPs/CLT may show improved therapeutic efficacy *in vivo*.

Next, to explore the therapeutic efficacy of NNPs/CLT *in vivo*, we established both a Panc02 tumor bearing xenograft mice model and an orthotopic GFP-Panc02 mice model. The selective accumulation of NNPs/DiD and NPs/DiD at the tumor site following systemic administration is likely mediated by the enhanced permeability and retention effect. Moreover, the enhanced accumulation of NNPs/DiD at the tumor site may be attributed to the enhanced cell uptake efficiency of NNPs/DiD in Panc02 cells. Regarding antitumor efficacy *in vivo*, NNPs/CLT have been proven to significantly inhibit tumor growth as compared to CLT solution or NPs/CLT thus further indicating improved therapeutic efficacy of NNPs/CLT in both ectopic and orthotopic tumor models. According to the literature, a blood–pancreas barrier has remained the major biological barrier for efficient delivery of therapeutics to the pancreas following systemic

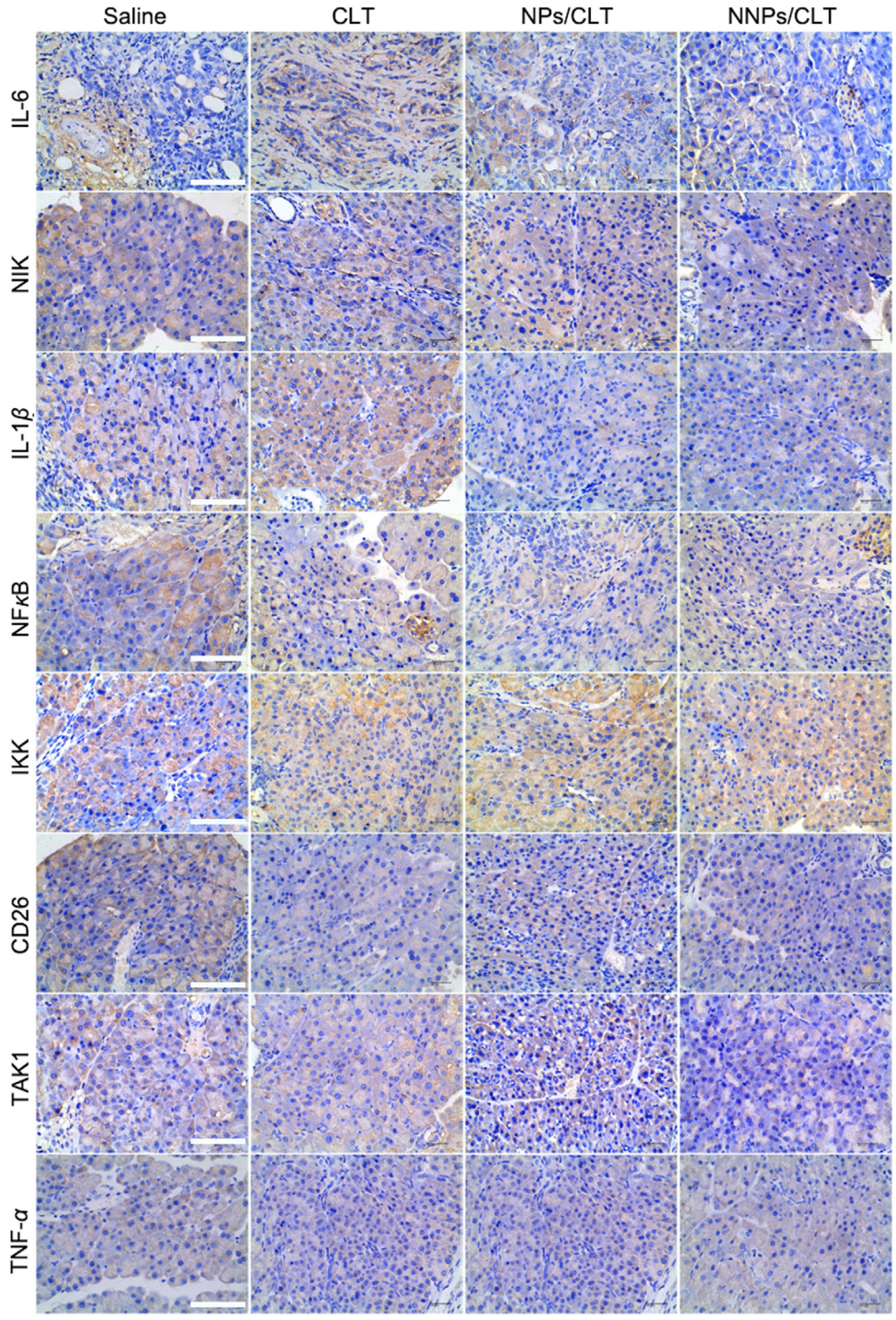

Figure 9 Immunohistochemistry of IL-6, NIK, IL-1β, NF-κB, IKK, CD126, TAK1 and TNF-α staining of tumor sections in the ectopic pancreatic cancer model. Scale bar = 100 μm.

administration[50,51]. which often resulted in the limited drug distribution in the pancreas thus a lack of therapeutic efficacy *in vivo*. Two strategies have been reported to achieve pancreas targeted drug delivery[52–54]: i) small molecule ligands were introduced *via* chemical modification to afford drug-ligand conjugates; ii) nanoscale delivery systems with targeting ligands, *e.g.*, nanoparticles were modified with peptides, antibodies or antibody fragments to afford targetability. Although chemical conjugation can help improve drug distribution in the pancreas, it usually involves multiple synthesis steps. Similarly, nanoscale delivery systems with active targeting ligands also involve complex processing technology and high cost of manufacturing, despite the advantages of enhanced pancreas-specific drug delivery[55,56]. Herein, neutrophil membrane-coated nanoparticles offer a unique technology to render polymeric nanoparticles biomimicking properties, which are well demonstrated to overcome the blood–pancreas barrier to achieve pancreas-specific drug delivery *in vivo*.

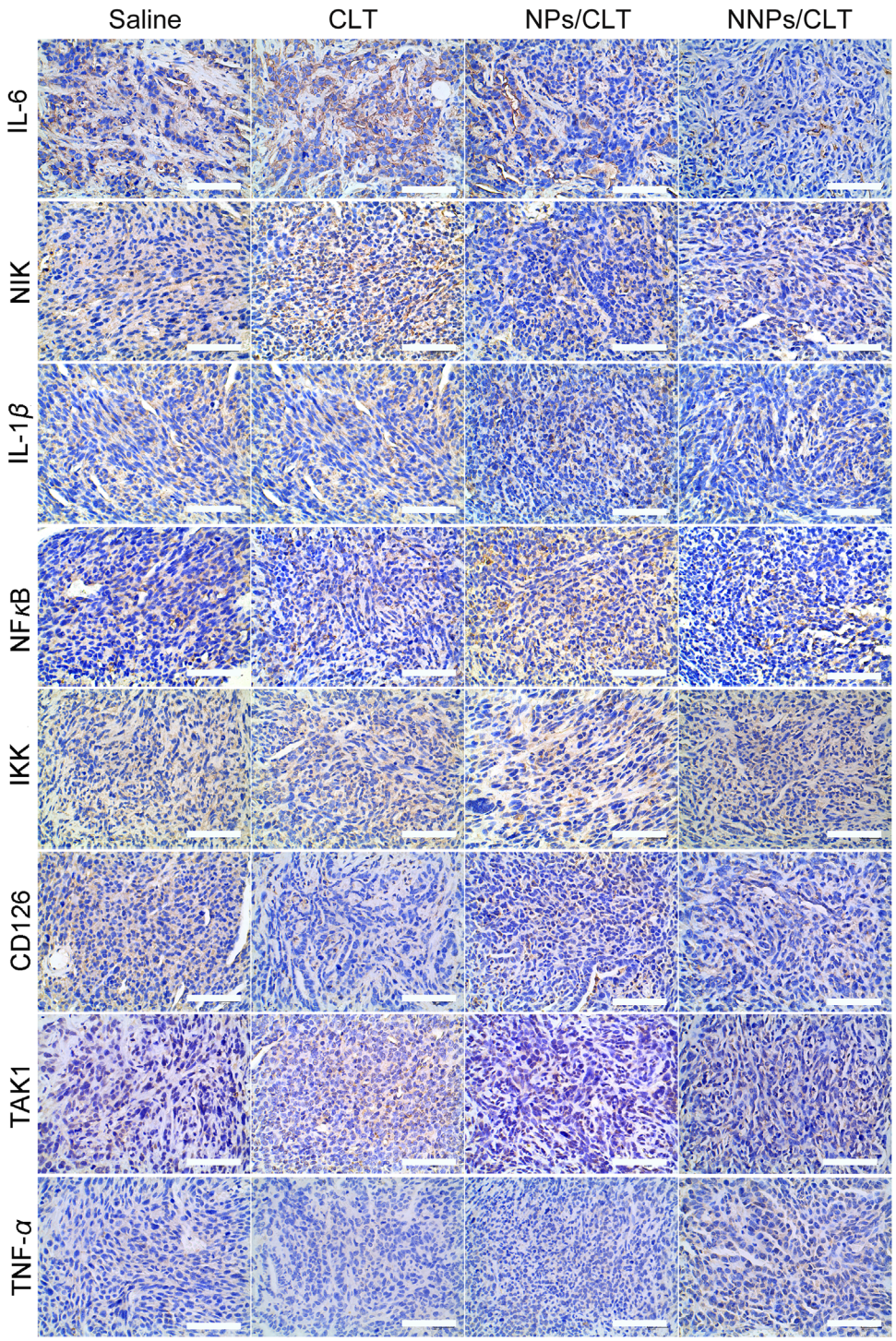

Figure 10 Immunohistochemistry of IL-6, NIK, IL-1β, NF-κB, IKK, CD126, TAK1 and TNF-α staining of tumor sections in the orthotopic pancreatic tumor mice model. Scale bar = 100 μm.

Clinically, the therapeutic efficacy of a drug is often limited due to a lack of site-specific distribution, and the "off-target" distribution to vital organs may cause systemic toxicity. Neutrophil membrane-coated nanoparticles have shown enhanced tumor-specific distribution in Panc02 tumor bearing mice xenograft model, which suggests coating nanoparticles with neutrophil membrane render nanoparticles the affinity to tumor cells. Moreover, coating polymeric nanoparticles with neutrophil membrane may greatly decrease the immunogenicity of synthetic nanoparticles following systemic administration thus improving the biocompatibility of these nanoparticles.

The pharmacological effect of CLT has been well validated in several studies, which is suggested to mainly function by inhibiting NF-κB signaling pathway[57,58]. As NF-κB is actively involved in the proliferation of cancer cells, the inhibition of NF-κB may thus result in anti-proliferation and pro-apoptosis effects[59,60].

Among all treatment groups, the level NF-κB in the tumor sections was significantly reduced in the NNPs/CLT treated group (Figs. 9 and 10). Furthermore, NNPs/CLT showed less cardiotoxicity compared to CLT solution and no significant damages to vital organs following systemic administration, which represents a viable delivery vehicle with targeting efficiency and safety. Despite improved inhibition effect against primary tumors, NNPs/CLT significantly minimized liver metastases in the orthotopic tumor model as compared to CLT solution and NPs/CLT. The anti-metastasis effect of NNPs may result from targeting the circulating cancer cells as previously reported[22].

5. Conclusions

We have developed naïve neutrophil membrane-coated PEG-PLGA nanoparticles to achieve pancreas-specific delivery of therapeutic compounds by overcoming the blood–pancreas barrier. A naturally derived compound, celastrol, was well proven to show excellent anticancer efficacy in both the ectopic and orthotopic pancreatic carcinoma animal models. Overall, NNPs/CLT selectively delivered to the disease site in pancreas achieved site-specific release of CLT, which then functions through down-regulating a series of pro-inflammatory factors to impact the local disease environment and improve the therapeutic outcome.

Acknowledgments

The authors gratefully acknowledge the financial support from the National Natural Science Foundation of China (81690261), Sichuan University Fund for Excellent Young Scholars (2017SCU04A23, China) and Sichuan Youth Science and Technology Innovation Research Team Funding (2016TD0001, China).

Appendix A. Supporting information

Supplementary data associated with this article can be found in the online version at https://doi.org/10.1016/j.apsb.2018.12.009.

References

1. Ryan DP, Hong TS, Bardeesy N. Pancreatic adenocarcinoma. *N Engl J Med* 2014;**371**:1039–49.
2. Peery AF, Crockett SD, Barritt AS, Dellon ES, Eluri S, Gangarosa LM, et al. Burden of gastrointestinal, liver, and pancreatic diseases in the United States. *Gastroenterology* 2015;**149**:1731–41.e.
3. Kamisawa T, Wood LD, Itoi T, Takaori K. Pancreatic cancer. *Lancet* 2016;**388**:73–85.
4. Sato N, Cheng XB, Kohi S, Koga A, Hirata K. Targeting hyaluronan for the treatment of pancreatic ductal adenocarcinoma. *Acta Pharm Sin B* 2016;**6**:101–5.
5. Zhang SH, Zhang H, He HW, Li Y, Li XY, Zhang LF, et al. *In vivo* real-time imaging of gemcitabine-leaded growth inhibition in the orthotopic transplantation model of human pancreatic tumor. *Acta Pharm Sin B* 2011;**1**:220–5.
6. Bond-Smith G, Banga N, Hammond TM, Imber CJ. Pancreatic adenocarcinoma. *Br Med J* 2012;**344**:1–10.
7. Vincent A, Herman J, Schulick R, Hruban RH, Goggins M. Pancreatic cancer. *Lancet* 2011;**378**:607–20.
8. Seufferlein T, Bachet JB, van Cutsem E, Rougier P, Grp EGW. Pancreatic adenocarcinoma: esmo-esdo clinical practice guidelines for diagnosis, treatment and follow-up. *Ann Oncol* 2012;**23**:33–40.
9. Jura N, Archer H, Bar-Sagi D. Chronic pancreatitis, pancreatic adenocarcinoma and the black box in-between. *Cell Res* 2005;**15**:72–7.
10. Greten FR, Eckmann L, Greten TF, Park JM, Li ZW, Egan LJ, et al. IKKβ links inflammation and tumorigenesis in a mouse model of colitis-associated cancer. *Cell* 2004;**118**:285–96.
11. Coussens LM, Werb Z. Inflammation and cancer. *Nature* 2002;**420**:860–7.
12. Luo S, Li PW, Li S, Du ZW, Hu X, Fu Y, et al. *N,N*-Dimethyl tertiary amino group mediated dual pancreas- and lung-targeting therapy against acute pancreatitis. *Mol Pharm* 2017;**14**:1771–81.
13. Karin M, Cao YX, Greten FR, Li ZW. NF-κB in cancer: from innocent bystander to major culprit. *Nat Rev Cancer* 2002;**2**:301–10.
14. Algul H, Tando Y, Schneider G, Weidenbach H, Adler G, Schmid RM. Acute experimental pancreatitis and NF-κB/Rel activation. *Pancreatology* 2002;**2**:503–9.
15. Kang T, Gao XL, Hu QY, Jiang D, Feng XY, Zhang X, et al. iNGR-modified PEG-PLGA nanoparticles that recognize tumor vasculature and penetrate gliomas. *Biomaterials* 2014;**35**:4319–32.
16. El-Tanbouly GS, El-Awady MS, Megahed NA, Salem HA, El-Kashef HA. The NF-κB inhibitor celastrol attenuates acute hepatic dysfunction induced by cecal ligation and puncture in rats. *Environ Toxicol Pharmacol* 2017;**50**:175–82.
17. Zhang YL, Geng C, Liu XY, Li MX, Gao MY, Liu XJ, et al. Celastrol ameliorates liver metabolic damage caused by a high-fat diet through SIRT1. *Mol Metab* 2017;**6**:138–47.
18. Guo L, Luo S, Du ZW, Zhou ML, Li PW, Fu Y, et al. Targeted delivery of celastrol to mesangial cells is effective against mesangioproliferative glomerulonephritis. *Nat Commun* 2017;**8**:1–17.
19. Chen SR, Dai Y, Zhao J, Lin LG, Wang YT, Wang Y. A mechanistic overview of triptolide and celastrol, natural products from *Tripterygium wilfordii* hook f. *Front Pharmacol* 2018;**9**:1–13.
20. Ricchi P, Zarrilli R, di Palma A, Acquaviva AM. Nonsteroidal anti-inflammatory drugs in colorectal cancer: from prevention to therapy. *Br J Cancer* 2003;**88**:803–7.
21. Zerbini LF, Tamura RE, Correa RG, Czibere A, Cordeiro J, Bhasin M, et al. Combinatorial effect of non-steroidal anti-inflammatory drugs and NF-κB inhibitors in ovarian cancer therapy. *PLoS One* 2011;**6**:1–11.
22. Gash KJ, Chambers AC, Cotton DE, Williams AC, Thomas MG. Potentiating the effects of radiotherapy in rectal cancer: the role of aspirin, statins and metformin as adjuncts to therapy. *Br J Cancer* 2017;**117**:210–9.
23. Xue JW, Zhao ZK, Zhang L, Xue LJ, Shen SY, Wen YJ, et al. Neutrophil-mediated anticancer drug delivery for suppression of postoperative malignant glioma recurrence. *Nat Nanotechnol* 2017;**12**:692–700.
24. Kang T, Zhu QQ, Wei D, Feng JX, Yao JH, Jiang TZ, et al. Nanoparticles coated with neutrophil membranes can effectively treat cancer metastasis. *ACS Nano* 2017;**11**:1397–411.
25. Li RX, He YW, Zhang SY, Qin J, Wang JX. Cell membrane-based nanoparticles: a new biomimetic platform for tumor diagnosis and treatment. *Acta Pharm Sin B* 2018;**8**:14–22.
26. Luk BT, Zhang LF. Cell membrane-camouflaged nanoparticles for drug delivery. *J Control Release* 2015;**220**:600–7.
27. Wu ZG, Li TL, Gao W, Xu TL, Jurado-Sanchez B, Li JX, et al. Cell-membrane-coated synthetic nanomotors for effective biodetoxification. *Adv Funct Mater* 2015;**25**:3881–7.
28. Gao WW, Zhang LF. Engineering red-blood-cell-membrane-coated nanoparticles for broad biomedical applications. *Aiche J* 2015;**61**:738–46.
29. Fang RH, Luk BT, Hu CMJ, Zhang LF. Engineered nanoparticles mimicking cell membranes for toxin neutralization. *Adv Drug Deliv Rev* 2015;**90**:69–80.
30. Chen BY, Luo M, Liang JM, Zhang C, Gao CF, Wang J, et al. Surface modification of PGP for a neutrophil–nanoparticle co-vehicle to enhance the anti-depressant effect of baicalein. *Acta Pharm Sin B* 2018;**8**:64–73.
31. Hu X, Jia MD, Fu Y, Zhang P, Zhang ZR, Lin Q. Novel low-toxic derivative of celastrol maintains protective effect against acute renal injury. *ACS Omega* 2018;**3**:2652–60.

32. Wilhelmsen K, Farrar K, Hellman J. Quantitative *in vitro* assay to measure neutrophil adhesion to activated primary human microvascular endothelial cells under static conditions. *J Vis Exp* 2013:1–8.
33. Du X, Nyagblordzro M, An LJ, Gao X, Du LM, Wang YY, et al. Pharmacokinetic and toxicological characteristics of tripterigium glycosides and their derivatives. *Curr Drug Metab* 2018;**19**:605–27.
34. Higuchi T, Yokobori T, Naito T, Kakinuma C, Hagiwara S, Nishiyama M, et al. Investigation into metastatic processes and the therapeutic effects of gemcitabine on human pancreatic cancer using an orthotopic SUIT-2 pancreatic cancer mouse model. *Oncol Lett* 2018;**15**:3091–9.
35. Huang HC, Rizvi I, Liu J, Anbil S, Kalra A, Lee H, et al. Photodynamic priming mitigates chemotherapeutic selection pressures and improves drug delivery. *Cancer Res* 2018;**78**:558–71.
36. Pang XF, Yi ZF, Zhang J, Lu BB, Sung B, Qu WJ, et al. Celastrol suppresses angiogenesis-mediated tumor growth through inhibition of AKT/mammalian target of rapamycin pathway. *Cancer Res* 2010;**70**:1951–9.
37. Zhao Y, Tan YN, Meng TT, Liu X, Zhu Y, Hong Y, et al. Simultaneous targeting therapy for lung metastasis and breast tumor by blocking the NF-κB signaling pathway using celastrol-loaded micelles. *Drug Deliv* 2018;**25**:341–52.
38. Petronelli A, Pannitteri G, Testa U. Triterpenoids as new promising anticancer drugs. *Anti-Cancer Drugs* 2009;**20**:880–92.
39. Li-Weber M. Targeting apoptosis pathways in cancer by chinese medicine. *Cancer Lett* 2013;**332**:304–12.
40. Lukaszewicz-Zajac M, Mroczko B, Kozlowski M, Niklinski J, Laudanski J, Szmitkowski M. Higher importance of interleukin 6 than classic tumor markers (carcinoembryonic antigen and squamous cell cancer antigen) in the diagnosis of esophageal cancer patients. *Dis Esophagus* 2012;**25**:242–9.
41. Verma G, Bhatia H, Datta M. Gene expression profiling and pathway analysis identify the integrin signaling pathway to be altered by IL-1β in human pancreatic cancer cells: role of JNK. *Cancer Lett* 2012;**320**:86–95.
42. Cacev T, Kapitanovic S. Interleukin-6 mRNA expression in sporadic colon cancer. *Inflamm Res* 2007;**56**:S460.
43. Jin S, Mutvei AP, Chivukula IV, Andersson ER, Ramskold D, Sandberg R, et al. Non-canonical notch signaling activates IL-6/JAK/STAT signaling in breast tumor cells and is controlled by p53 and IKKα/IKKβ. *Oncogene* 2013;**32**:4892–902.
44. Agarwal A, Fukuyama R, Lerner N, Kelleher C, Sizemore N. The IKK/NF-κB & β-catenin pathway is critical for migration, invasion and metastasis in colorectal cancer. *Cancer Res* 2006;**66**.
45. Tao ZM, Muzurndar MD, Detappe A, Huang X, Xu ES, Yu YJ, et al. Differences in nanoparticle uptake in transplanted and autochthonous models of pancreatic cancer. *Nano Lett* 2018;**18**:2195–208.
46. Kolaczkowska E, Kubes P. Neutrophil recruitment and function in health and inflammation. *Nat Rev Immunol* 2013;**13**:159–75.
47. Zarbock A, Ley K, McEver RP, Hidalgo A. Leukocyte ligands for endothelial selectins: specialized glycoconjugates that mediate rolling and signaling under flow. *Blood* 2011;**118**:6743–51.
48. Petri B, Phillipson M, Kubes P. The physiology of leukocyte recruitment: an *in vivo* perspective. *J Immunol* 2008;**180**:6439–46.
49. Chu DF, Gao J, Wang ZJ. Neutrophil-mediated delivery of therapeutic nanoparticles across blood vessel barrier for treatment of inflammation and infection. *ACS Nano* 2015;**9**:11800–11.
50. Gong-Hua LI, Jin-Wen QI, Ke MA. Transference of tinidazole across the blood–pancreas barrier in rats. *Herald Med* 2006;**25**:858–60.
51. Ma KMK, Qi JQJ, Yu JYJ, Jin GJG, Zhao DZD, Jiang WJW, et al. Penetration of lovofloxacin in blood–pancreatic barrier in rats. *Chin J Mod Appl Pharm* 2002;**19**:237–9.
52. Arlt A, Muerkoster SS, Schafer H. Targeting apoptosis pathways in pancreatic cancer. *Cancer Lett* 2013;**332**:346–58.
53. Gogate PN, Kurenova EV, Ethirajan M, Liao JQ, Yemma M, Sen A, et al. Targeting the c-terminal focal adhesion kinase scaffold in pancreatic cancer. *Cancer Lett* 2014;**353**:281–9.
54. Craven KE, Gore J, Korc M. Overview of pre-clinical and clinical studies targeting angiogenesis in pancreatic ductal adenocarcinoma. *Cancer Lett* 2016;**381**:201–10.
55. Murata M, Narahara S, Kawano T, Hamano N, Piao JS, Kang JH, et al. Design and function of engineered protein nanocages as a drug delivery system for targeting pancreatic cancer cells *via* neuropilin-1. *Mol Pharm* 2015;**12**:1422–30.
56. Shen M, Xu YY, Sun Y, Han BS, Duan YR. Preparation of a thermosensitive gel composed of a MPEG-PLGA-PLL-cRGD nano-drug delivery system for pancreatic tumor therapy. *ACS Appl Mater Interfaces* 2015;**7**:20530–7.
57. Maier HJ, Schmidt-Strassburger U, Huber MA, Wiedemann EM, Beug H, Wirth T. NF-κB promotes epithelial-mesenchynmal transition, migration and invasion of pancreatic carcinoma cells. *Cancer Lett* 2010;**295**:214–28.
58. Bao B, Wang ZW, Ali S, Kong DJ, Li YW, Ahmad A, et al. Retracted: notch-1 induces epithelial–mesenchymal transition consistent with cancer stem cell phenotype in pancreatic cancer cells (retracted article. See vol. 423, pg. 153, 2018). *Cancer Lett* 2011;**307**:26–36.
59. Prasad R, Katiyar SK. Grape seed proanthocyanidins inhibit migration potential of pancreatic cancer cells by promoting mesenchymal-to-epithelial transition and targeting NF-κB. *Cancer Lett* 2013;**334**:118–26.
60. Kong R, Sun B, Jiang HC, Pan SH, Chen H, Wang SJ, et al. Downregulation of nuclear factor-κB p65 subunit by small interfering RNA synergizes with gemcitabine to inhibit the growth of pancreatic cancer. *Cancer Lett* 2010;**291**:90–8.